Theoretical prediction of the punching shear strength of concrete flat slabs under in-plane tensile forces

Pablo G. Fernández, Antonio Marí and Eva Oller

Civil and Environmental Engineering Department. Universitat Politècnica de Catalunya (UPC), Barcelona, Spain

Engineering Structures 229 (2021), https://doi.org/10.1016/j.engstruct.2020.111632
Received 15 May 2020; Received in revised form 26 October 2020; Accepted 18 November 2020 0141-0296/

ABSTRACT

RC slabs can be subjected simultaneously to transverse loads and in-plane tensile forces, as it happens in top slabs of continuous box girder bridges decks, in the regions of negative moments, or in flat slabs subjected to horizontal loads, produced by wind or earth pressure. Tensile forces can reduce the shear punching capacity of slabs. However, few studies have been carried out to quantify this effect. With this purpose, a mechanical model has been developed to capture the influence of in-plane tensile forces on the punching shear strength and verified with punching tests under different in-plane tensile load levels. The model, presented in this paper, consists of an extension of the Punching shear Compression Chord Capacity Model to account for the effects of tensile forces on the resisting actions. A linear reduction of the punching shear strength as a function of the external load applied has been obtained for moderate tensile forces, whereas high level of tensile forces may produce premature yielding of the reinforcement and further reduction of the punching shear strength. The proposed model accurately captures the available test results, including the effects of the premature yielding of reinforcement when the tensile force produces concrete cracking. In addition, predictions of punching-shear-tensile tests available in the literature were made with different theoretical models included in design codes, which yielded in general conservative results and showed high scatter.

KEYWORDS. Punching shear, tension, slabs, mechanical model, reinforced concrete, yielding, cracking

NOTATION

a: Shear span. For slabs floors in buildings subjected to distributed loads, the shear span a, to be used in the size effect parameter ζ, can be estimated as the average distance from the position of the line of zero radial bending moment to the edge of the column, $l_0 = \sqrt{l_{0x} \cdot l_{0y}}$, where $l_{0x} \approx 0.22 \cdot l_x$ *and* $l_{0y} \approx 0.22 \cdot l_y$. are the span lengths in the x and y directions.

A_c: Concrete cross-sectional area of the slab

b_0: Shear-resisting control perimeter, according to Model Code 2010

b_1',b_2': Portion of the control perimeter considered in each orthogonal direction, according to ACI 349-06

b_w: Width of the web on T, I or L beams. For rectangular beams or slabs, $b_w = b$

C: Compression force acting on the control section of the slab

d: Effective depth of the cross-section

d_0: Effective depth of the cross-section d, but not less than 100 mm

d_g: Largest nominal maximum aggregate size

d_l: Effective depth of the cross-section subjected to tension

d_t: Effective depth of the cross-section not subjected to tension

d_v: Shear-resisting effective depth of the slab according to Model Code 2010

f_c: Concrete compressive strength

f_{ck}: Characteristic concrete compressive strength

f_{cc}: Confined concrete compressive strength

f_{ct}: Tensile strength of concrete

f_y: Yield stress of the reinforcement

f_y*: Reduced yield stress of the reinforcement due to tensile stresses

h: Height of the slab's cross-section

k_c: Relative neutral axis depth (x/d). No less than 0.2

k_{dg}: Factor to account for the maximum aggregate size on the shear strength

k_ψ: Factor to account for the rotations of the slab on the shear strength

m_{cr}: Slab's cracking bending moment per unit width considering T=0

M: Acting bending moment on the control section of the slab

m: Acting bending moment on the control section of the slab, per unit length

m_r: Bending moment per unit length producing radial stresses around the column

m_φ: Bending moment per unit length producing tangential stresses around the column

r_0: Radial distance from the edge of the column to the point of zero radial bending moment

r_{crack}: Distance from the starting point of the critical crack (due to bending) to the column axis

r_{crit}: Distance from the control perimeter to the column axis

r_s: Distance between the point of zero radial bending moment and the column axis, according to Model Code 2010

T: External tensile force

Tcr: Tensile force associated to the section cracking in pure tension

t: Design tensile force per unit length

u_{crit}: Control perimeter, placed at a distance 0,5d from the column face

V_R: Punching-Shear resistance of the member considering T = 0

v_R: dimensionless form of V_R

V_c: Shear resisted in the un-cracked compression head considering T = 0

v_c: dimensionless form of V_c

$V_{R,t}$: Shear resistance of the member in the presence of in-plane tensile force

$v_{R,t}$: dimensionless form of $V_{R,t}$

V_{ct}: Shear force resisted by the compression chord, in the presence of in-plane tensile force

v_{ct}: dimensionless form of V_{ct}

$V_{R,t/2}$: Shear resistance of the member in the presence of unidirectional in-plane tensile forces

V_y: Punching strength associated to reinforcement yielding

x_0: Neutral axis depth considering T = 0

x: Neutral axis depth

z: Inner lever arm. The approximate value of z = 0.9d may normally be used

β: Horizontal projection of the first branch of the critical crack

ζ: Size effect, defined in (7)

θ: Inclination of the critical crack

v: Poisson's coefficient

ρ: Reinforcement ratio. The neutral axis depth should be obtained using the average of the longitudinal reinforcement ratios ρ_l and ρ_t in the two orthogonal directions

σ_1: Maximum principal stress in the r-z plane

σ_2: Minimum principal stress in the r-z plane

σ_{cp}: Average value of the normal concrete stresses in the critical section in the two orthogonal directions (positive in compression)

σ_r: Normal radial stresses around the column produced by m_r

σ_φ: Normal tangential stresses around the column produced by m_φ

σ_z: Vertical stresses in the slab in the vicinity of the column

ψ: Rotation of the slab at failure, according to Model Code 2010

1. Introduction

RC slabs subjected to the simultaneous action of transverse concentrated loads and in-plane tensile forces can be found in continuous box girder bridges, at intermediate supports, where tensile stresses arise in top slab, as a result of hogging bending moments, and may act together with a heavy vehicle load. Another common situation where this phenomenon takes place is on floor slabs supported on columns and subjected to a horizontal load, due to wind or earth pressure, on one of their sides. Skew compression fields going from the loaded side to the restraining columns of the opposite side may generate tensile stresses in the perpendicular direction, as can be seen in Fig. 1.

Figure 1

In-plane axial forces may arise also from restrained imposed deformations, such as shrinkage of concrete or thermal strains, either due to cooling after setting or due to environmental thermal effects, which may produce cracks in the concrete and, therefore, reduce the punching shear strength of the slab.

The phenomenon of punching shear has been extensively studied over the years, both theoretically and experimentally [1-15]. However, few studies have been carried out regarding punching shear when there are tensile forces in the mid-plane of the slabs, so that further research is needed to quantify the effects of such forces on the punching shear strength of the slabs.

Two experimental campaigns were carried out at Cornell University [16-17] in the late ’70 and early ’80, in the context of an investigation for the U.S Nuclear Regulatory Commission, where several 1.2 x 1.2 x 0.150 m reinforced concrete slabs subjected to bi-axial tension (Fig. 2-c) were tested in punching. In the same period of time, P.E. Regan, in his report entitled “Punching shear

123 in prestressed concrete slab bridges" [18], presents the results of three 1.5 x 1.5 x 0.125 m slabs
124 (BD Series) subjected to unidirectional in-plane tension and an out-of-plane concentrated load on
125 its center, all of them with different support scheme (Fig .2-a), but only one of them can be
126 considered a two way slab (BD-6). Experimental studies have been also carried out by Bui et al
127 [19], regarding the influence of uniaxial tension on the shear strength of 2.6 x 4 x 0.3 m simply
128 supported concrete slabs subjected to concentrated loads close to the support (Fig. 2-b). All these
129 studies concluded that axial tensile stresses reduce punching and shear strength respectively.
130
131 Figure 2
132
133 Punching shear provisions included in the most frequently used design codes, such as EC-
134 2 [20], ACI [21-22] or Model Code 2010 [23], contemplate the effect of in-plane normal stresses
135 in a different way. EC-2, in section 6.4.4, includes the effect of axial stresses on punching shear
136 strength by including the term $k_1 \cdot \sigma_{cp}$, in Eq. (1), with $\sigma_{cp} = N_u/A_c$, being N_u the axial load applied
137 in the cross-section, with negative sign in the case of tension. However, EC-2 considers that the
138 increment of punching shear strength due to a compression force C is equal to the reduction in
139 punching shear strength due to a tensile force of the same magnitude. However, the response of
140 concrete in one case or in the other one is radically different.

$$V_{Rd,c} = (C_{Rd,c} \cdot k \cdot \sqrt[3]{100 \cdot \rho_l \cdot f_{ck}} + k_1 \cdot \sigma_{cp}) \cdot u_1 \cdot d \quad (1)$$

141 ACI 318-14 "Building code requirements for structural concrete" [21], in section 22.6.5
142 (two-way shear) proposes two expressions to calculate the punching shear strength of a slab with
143 an axial compression load due to prestressing, but it does not mention the case of axial tension.
144 In section 22.7.5 (one-way shear), it proposes an expression for the shear strength of members
145 subjected to "significant" axial tension, Eq. (2), but what "significant" means is left to the
146 judgement of the designer. In Eq. (2), N_u is considered negative.

$$V_c = 0.17 \cdot \left(1 + \frac{N_u}{3.5 \cdot A_c}\right) \cdot \sqrt{f_c} \cdot \; b_w \;\; d \quad (2)$$

147 However, ACI 349-06 “Code Requirements for Nuclear Safety Concrete Structures” [22],
148 in section 11.12 provides a particular expression for the punching strength of slabs subjected to
149 membrane stresses. According to this code, the punching strength V_c, is equal to the sum of the
150 strength in each one of the two considered orthogonal directions V_{c1} and V_{c2}. The expression for
151 V_{c1} and V_{c2} are given in Eqs. (3a) - (3d), where β_c is a constant depending on the shape of the
152 column, f_m is the membrane stress and b_1' and b_2' are the portions of the control perimeter
153 considered in each direction. In the case of tensile membrane stresses, f_m is considered negative.

$$V_{c1} = \left(2 + \frac{4}{\beta_c}\right) \cdot \left(1 + \frac{0.25 \cdot f_{m1}}{\rho_1 \cdot f_y}\right) \cdot \sqrt{f_c} \cdot b_1' \cdot h \quad if \quad f_{m1} \leq 0.9 \cdot \rho_1 \cdot f_y \tag{3a}$$

$$V_{c1} = 0.5 \cdot \sqrt{f_c} \cdot h \quad if \quad f_{m1} > 0.9 \cdot \rho_1 \cdot f_y \tag{3b}$$

$$V_{c2} = \left(2 + \frac{4}{\beta_c}\right) \cdot \left(1 + \frac{0.25 \cdot f_{m2}}{\rho_2 \cdot f_y}\right) \cdot \sqrt{f_c} \cdot b_2' \cdot h \quad if \quad f_{m2} \leq 0.9 \cdot \rho_2 \cdot f_y \tag{3c}$$

$$V_{c2} = 0.5 \cdot \sqrt{f_c} \cdot h \quad if \quad f_{m2} > 0.9 \cdot \rho_2 \cdot f_y \tag{3d}$$

$$V_c = V_{c1} + V_{c2} \tag{3e}$$

154

155 Finally, Model Code 2010 [23], in section 7.3.5.3, presents the following expression for
156 the punching strength of slabs, based on the Critical Shear Crack Theory [11] (Eq. 4):

$$V_{Rd,c} = k_\psi \cdot \frac{\sqrt{f_{ck}}}{\gamma_c} \cdot b_0 \cdot \ d_v \tag{4}$$

157 This equation includes the term k_ψ, which depends on the rotation of the slab, ψ. Therefore,
158 it is different under compression or tension axial forces:

$$k_\psi = \frac{1}{1.5 + 0.9\, k_{dg}\, \psi\, d} \leq 0.6 \tag{5}$$

159 where k_{dg} depends on the aggregate size, d_g, whose value is $k_{dg} = 1$ for $d_g \geq 16$mm and $k_{dg} =$
160 $32/(16+ d_g) \geq 0.75$ for $d_g \leq 16$mm. To obtain ψ, MC-2010 proposes four levels of approximation
161 (LoA): levels I, II and III provide different analytical expressions to estimate the rotation ψ, while

level IV proposes to obtain the load-rotation curve by means of non-linear analysis including cracking, tension stiffening and yielding of the reinforcement.

In this context, an experimental campaign was carried out by the authors at the Laboratory of Technology of Structures and Materials of the Universitat Politècnica de Catalunya (UPC) [24]. The main objective of this program was to identify and quantify the effect of unidirectional in-plane tensile forces on the punching shear strength of reinforced concrete slabs. On the other hand, it was intended to provide experimental results to contribute to extend the mechanically-based punching shear resistance model "Compression Chord Capacity Model" (CCCM) [25], developed by some of the authors, to the case of in-plane tension. Results of this campaign showed a progressive reduction of the punching shear strength with an increment of the tensile stresses in acting in the slab cross section, which is in good agreement with the results of the above-mentioned previous research.

The main goal of this paper is to present the extension of the punching shear CCCM model to account for the effects of in-plane tensile stresses. The fundamentals of the modifications carried out are explained and new equations are derived and validated with the results of the experimental campaigns on punching shear tests carried out at Cornell University [16-17] and at UPC, [24] whose main characteristics will be briefly explained later in sections 3 and 4 of this paper. In addition, a comparison of the predictions of the available tests results using the proposed model and the above mentioned theoretical models is also presented.

2. Proposed mechanical model for punching shear with in-plane tensile forces

2.1 Brief summary of the Compression Chord Capacity Model for shear and punching shear

The Compression Chord Capacity Model (CCCM) [26] is a shear strength mechanical model derived from a more general model called Multi-Action Shear Model (MASM), developed by Marí et al. [27]. As it is widely accepted, such model considers that the shear strength (V_R) is composed by the shear resisted in the un-cracked compression head (V_c), the shear resisted across the web cracks, by aggregate interlock and residual stresses (V_w) [28, 29], the shear resisted by the longitudinal reinforcement, due to dowel action (V_l), and the shear resisted by the transverse

reinforcement (V_s), providing explicit expressions for each component. The CCCM model join the three first components into a single one, V_c, called concrete contribution.

Distributions of normal and shear stresses are assumed by combining beam and arch effects, so that the compression chord is subject to a biaxial stress state. It is considered that failure occurs when the principal stresses at one point of the compression chord, at a critical section defined in [26] and [27], reach the Kupfer and Gerstle's biaxial failure envelope [30], in the compression-tension branch. To obtain the beam shear strength, equilibrium of forces and moments is set between the internal forces (V, M) and the stress resultants (Fig. 3) at the concrete chord (C, V_c), along the crack (V_w), at the stirrups (V_s) and at the longitudinal reinforcement (T, V_l). The rigid body considered for the equilibrium is that placed above the critical crack, from its initiation to the section where the crack reaches the neutral axis depth. Then, relating forces with stresses and taking into account the failure criterion, the ultimate shear force is obtained.

Figure 3

This model was extended to punching shear [25], taking into account the main differences between both phenomena, in order to incorporate them into the mechanical model. First, the position and inclination of the critical crack were formulated, taking into account the shape of radial bending moments law $m_r(r)$, and the position of the control perimeter was obtained, resulting an average value of the distance to the column face of 0.5d, being *"d"* the effective depth of the slab (Fig. 4-a). The second important effect faced was the multiaxial stress state in the slab compressed chord, due to vertical stresses in the vicinity of the column, enhancing the concrete capacity to resist shear stresses in the radial-vertical plane (Fig. 4-b). In addition, normal compressive stresses in the tangential direction also take place, thus increasing concrete strength in the radial plane. This phenomenon was incorporated in the model by modifying the compression-tension branch of Kupfer and Gerstle's biaxial failure envelope [30], using the confined concrete strength f_{cc}, from the EC-2 [21] formulation, instead of the unconfined strength f_c, so that a higher shear stress is needed to reach failure. Again, to obtain the punching shear

strength of the slab, the equilibrium between internal forces and stress resultants is taken in a portion of the slab placed under the critical crack, between the control perimeter (at a distance 0.5d from the column face) and the perimeter where the critical crack starts in the tension face (Fig. 4-c).

Solving the equilibrium equations, and assuming some simplifications explained in [25], the simplified expression for the punching shear strength, V_R, Eq. (6) is derived, where ζ is the size effect given by Eq. (7), u_{crit} is the control perimeter placed at a distance $s_{crit} = 0.5 \cdot d$ from the column face, and x_0/d is the relative neutral axis depth obtained assuming cracked concrete, zero tensile stresses and linear stress distribution in the compression chord.

Figure 4

$$V_R = 0.3 \cdot \zeta \left(1.125 \cdot \frac{x_0}{d} + 0.425\right) f_c^{2/3} \cdot u_{crit} \cdot d \tag{6}$$

$$\zeta = \frac{2\left(\frac{d}{a}\right)^{0.2}}{\sqrt{1 + {}^{d}/_{100}}} \geq 0.45 \tag{7}$$

Due to the internal redundancy of the slabs, yielding of the reinforcement and redistribution of moments may take place so that shear failure may occur without collapse. Assuming perfect plasticity, [25], for a point load, the punching strength associated to reinforcement yielding is given by Eq. (8).

$$V_R \leq V_Y \approx 2\pi f_y d^2 \left(1 - \frac{\rho f_y}{2 f_c}\right) \tag{8}$$

The ultimate punching shear strength should be the lowest value between those values obtained by Eqs. (6) and (8), but should not be lower than a minimum value punching shear strength, given by:

$$V_{R,min} = 0.3 \left[\zeta(1.125 k_c + 0.375) + \frac{10}{d_0}\right] f_c^{2/3} \cdot u_{cri} \cdot d \tag{9}$$

where $k_c = x/d \leq 0.2$, and $d_0 = \max(d; 100\text{mm})$. This minimum value corresponds to cases with very low longitudinal reinforcement ratio or depth, where the shear resisted along the cracked web

(V_w) is comparable to that resisted in the compression chord, since x_0/d is very small and V_w increases as the effective depth decreases [25].

2.2 Extension of the punching-shear CCCM to account for in plane tensile forces

To account for the influence of an in-plane tensile force on the ultimate load, the effects of such tensile force on the slab behavior and the equations affected by the force should be identified. These effects are at least the following:

1) The crack width increases due to the presence of a tensile force, so the aggregate interlock in the critical crack and, therefore, the shear resisted by the web, decreases. Such effect does not affect the assumption of the model of a very small web contribution.
2) The angle of inclination of the cracks, θ, may be affected by the presence of the tensile force, however this effect is considered to have little influence on the punching strength because it hardly affects the position of the control perimeter, and therefore, has not been taken into account in the proposed model.
3) The presence of a tensile force reduces the depth of the neutral axis, thus reducing the contribution of the compressed chord.
4) For a given bending moment, M, the tensile force decreases the compression stress in the un-cracked chord, thus reducing its ability to transmit shear stresses.
5) The axial tensile force increases the tensile stresses in the flexural reinforcement. Therefore, it is possible that for a tensile force that produces concrete cracking, a premature yielding takes place in the longitudinal reinforcement parallel to the tension direction.

The neutral axis depth x, in a section subjected to a bending moment, M, and an axial tensile force T, can be approached by the Eq. (10) [31]:

$$x = x_0 \left(1 - 0.1 \frac{T \cdot d}{M}\right) \tag{10}$$

Where d is the effective depth and x_0 is the neutral axis depth in pure flexure, without tensile force. The influence of the tensile force on the compression stress on the un-cracked concrete chord can

be obtained by including the tensile force in the equilibrium equations of a slice of slab (Eqs. 11 to 13), as indicated in Figure 5.

Figure 5

$$C = T_l + V_w \cdot \tan\theta - \mathrm{T} \tag{11}$$

$$\mathrm{V} = V_{ct} + V_w \tag{12}$$

$$C \cdot z + m_\varphi \cdot d\varphi \cdot \beta d = m_{cr}\frac{r_{crack}}{r_{crit}} + V_{ct}\beta d + V_w\beta_w d(1+\tan^2\theta) - 0.5 \cdot \mathrm{T} \cdot z \tag{13}$$

where the differential term $m_\varphi \cdot d\varphi \cdot \beta d$ due to the tangential moment can be neglected. The distance βd is the horizontal projection of the critical crack, in the tensile part of the slab, for which a value of $\beta = \frac{0.5\cdot\left(1-\frac{x}{d}\right)}{x/d}$ (Fig. 4-a) has been adopted, as in the punching-shear model [25]. V_w is the vertical resultant of the residual tensile stresses through the critical crack, which are very small when the crack width is large. A horizontal lever arm of these forces $\beta_w d = 2d/3$ is conservatively adopted. Then, adopting as lever arm in flexure, $z = d\text{-}x/3$, the normal stress in the radial direction at the critical point of the un-cracked chord, located at a distance $\lambda = 0.425x$ from the neutral axis is:

$$\sigma_r(\lambda) = \frac{2\lambda C}{xz} = \frac{2\lambda(m_{cr}\frac{r_{crack}}{r_{crit}} + V_c\beta d + V_w\beta_w d(1+\tan^2\theta) - 0{,}5\mathrm{T}\left(d-\frac{x}{3}\right))}{x(d-\frac{x}{3})} \tag{14}$$

The fundamental equation of the model is the one that allows obtaining the shear stress at the critical point of the compressed chord where the damage is maximum. This corresponds to the point where the combination of principal stresses reaches the Kupfer failure envelope at the first time. Then, the shear force resisted by the compression chord, in the presence of in-plane tensile force, V_{ct}, is obtained by integration of the shear stresses, what is straightforward since their distribution is assumed to be parabolic, and can be expressed in a dimensionless form by:

$$v_{ct} = \frac{V_{ct}}{f_{ct}bd} = 0.682\zeta \cdot \frac{x}{d} \cdot \frac{\sigma_1}{f_{ct}}\sqrt{1 - \frac{\sigma_r+\sigma_z}{\sigma_1} + \frac{\sigma_r\sigma_z}{\sigma_1^2}} = 0.682\zeta\frac{x}{d}R_t\sqrt{1 - \frac{\sigma_r+\sigma_z}{f_{ct}\cdot R_t} + \frac{\sigma_r\sigma_z}{f_{ct}^2\cdot R_t^2}} \tag{15}$$

where ζ is the size effect given by Eq. (7), x/d is the neutral axis depth, and R_t is the ratio between the principal tensile stress and the tensile strength at the critical point, which is provided by the modified Kupfer and Gerstle's envelope equation in the tension-compression branch:

$$\frac{\sigma_1}{f_{ct}} + 0.8\frac{\sigma_2}{f_{cc}} = 1 \rightarrow R_t = \frac{\sigma_1}{f_{ct}} = (1 - 0.8\frac{\sigma_2}{f_{cc}}) \quad (16)$$

Equation (15) is solved iteratively, since R_t depends on the principal stresses, and these depend on the shear stress, which is not known a priori. Once v_{ct} is obtained, its value is plotted in function of x_0/d for different values of the ratio T/T_{cr}, where T is the in-plane tensile force and T_{cr} is the tensile force associated to the section cracking in pure tension (see Fig. 6). To calculate the total punching strength of the slab, $V_{R,t}$, the shear transferred across the crack V_w must be added to V_{ct}. As explained in [25], V_w is much smaller than V_{ct}, and an average minimum value of $v_w = V_w/(f_{ct} \cdot u_{cri} \cdot d) = 0.05$ has been considered.

Therefore, the total punching strength of a slab subjected to in-plane tension is very well approached by (17).

$$V_{R,t} = \mathrm{V}_{ct} + V_w = 0.3\zeta \left(\left(1.125 - 0.85\frac{T}{T_{cr}} \right) \frac{x_0}{d} + 0.425 \right) \cdot f_c^{2/3} \cdot u_{crit} \cdot d \quad (17)$$

In this equation, the tensile strength of concrete f_{ct}, used in Eqs. (15) and (16) has been expressed in terms of the compressive strength f_c, ζ is the size effect given by Eq. (7), and x_0/d is the neutral axis depth of the section in pure bending. It is observed that the higher the tensile force, the lower is the shear resisted. In addition, for $T = 0$, Eq. (17) provides the same shear strength as Eq. (6)

Figure 6

In the case of slabs subjected to tensile forces in one direction, Eq. (17) must be applied only to the part of the control perimeter affected by the tensile stresses, which is approximately half of the total perimeter (see Fig. 7).

307

308 Figure 7

309

310 In addition, in order to obtain the neutral axis depth under bending and tension (Eq. (10)),
311 the following values of the tensile force T and the bending moment per unit width, m, must be
312 used:

$$t = \frac{T}{2a} = \frac{T}{T_{cr}} \cdot \frac{T_{cr}}{2a} = \frac{T}{T_{cr}} \cdot \frac{f_{ct} \cdot 2a \cdot d}{2a} = \frac{T}{T_{cr}} f_{ct} \cdot d \tag{18}$$

$$m = m_{cr} = \frac{f_{ct} h^2}{6} = \frac{f_{ct} d^2}{6} \left(\frac{h}{d}\right)^2 \cong 0.2 f_{ct} d^2 \tag{19}$$

313 where t is the design tensile force per unit width, T is the design total force uniformly applied to
314 the slab, a is the shear span, which coincides with half of the width of the slab tested, T_{cr} is the
315 value of the external tensile force that produces cracking of the cross-section, d is the effective
316 depth and m_{cr} is the cracking moment per unit width, computed without considering any applied
317 tensile force, and assuming h/d = 1.1. Then, Eq. (10) can be rewritten as:

$$\frac{x}{d} = \frac{x_0}{d}\left(1 - 0.1 \frac{t \cdot d}{m_{cr}}\right) = \frac{x_0}{d}\left(1 - 0.1 \frac{T}{T_{cr}} \frac{f_{ct}.d^2}{0.2\, f_{ct}.d^2}\right) = \frac{x_0}{d}\left(1 - 0.5 \frac{T}{T_{\mathrm{cr}}}\right) \tag{20}$$

318 The shear resisted along the control perimeter in the unidirectional tension case, $V_{R,t/2}$, may
319 be estimated as the mean value of the shear force resisted in the faces affected and non-affected by
320 the tensile stresses, given by Eqs. (6) and (17), respectively [32].

$$V_{R,t/2} = \frac{V_R}{2} + \frac{V_{R,t}}{2} = 0.3\zeta\left(\left(1.125 - 0.425 \cdot \frac{T}{T_{cr}}\right) \cdot \frac{x_0}{d} + 0.425\right) \cdot f_c^{\,2/3} \cdot u_{crit} \cdot d \tag{21}$$

321 For values of $T > T_{cr}$, the contribution of the concrete to resist tension is not considered, being
322 the tensile force resisted only by the reinforcement, whose stress increases considerably. If the
323 longitudinal reinforcement yields, Eq. (8) applies. Then, the effect of in-plane tensile forces is
324 considered by using a reduced steel strength in the tension direction, given by:

$$f_y^* = f_{y-} \frac{T}{A_s} \tag{22}$$

Due to this reduction, the punching strength associated to reinforcement yielding, V_y, may become dominant, diminishing even more the strength and stiffness of the slab. Then, the punching shear strength of slabs subjected to in-plane tensile forces is given by the lower of the following values:

$$V_{R,t} = 0.3\,\zeta \left(\left(1.125 - 0.85 \frac{T}{T_{cr}} \right) \frac{x_0}{d} + 0.425 \right) f_c^{2/3}\, u_{crit}\, d \tag{23}$$

$$V_{R,t} \leq V_y \approx 2\pi f_y^* d^2 \left(1 - \frac{\rho f_y^*}{2 f_c} \right) \tag{24}$$

where f_y^* is given by Eq. (22). Figure 8 shows the influence of the longitudinal reinforcement ratio on the reduction of punching shear strength as T/T_{cr} increases in the case of unidirectional in-plane tensile forces, obtained from Eqs. (21) and (24). In case of uniaxial tension, if Eq. (24) is satisfied, $V_{R,t}$ has to be replaced by V_y in Eq. (21).

Figure 8

Fig. 8 shows that, in the uniaxial tension case, for higher reinforcement ratios parallel to the tensile force ($\rho_l \geq 0.014$), a linear reduction of punching shear strength takes place, since failure is governed by Eq. (23). However, as ρ_l decreases, for certain value of T/T_{cr}, the slope of the straight line (and the reduction of punching strength) is higher, since yielding of reinforcement takes place, prior to punching failure, being the punching strength governed by Eq. (24). This fact may happen even for $T<T_{cr}$, for low reinforcement ratios ($\rho_l < 0.011$). Furthermore, it can be observed that for $T=T_{cr}$, another change of slope takes place, since the slab is cracked under the tensile force, and a sudden increment of tensile stress in the reinforcement takes place. This fact occurs even for higher reinforcement ratios ($\rho_l \geq 0.014$), although in these cases the increment of stress is not relevant. Finally, a minimum punching strength is reached (bottom horizontal line) of value $V_{R,t/2}/V_R = 0.5$, which corresponds to the shear resisted by the portion of the control perimeter parallel to the tensile forces, not affected by tensile stresses. In case of a slab supported on a circular column, the tensile force per unit length normal to the control perimeter, and the

neutral axis depth, both depend on the angle φ (see figure 7). Then, in that case, the punching strength should be obtained by integration of the shear per unit length obtained for each value of the angle φ along the control perimeter. However, parametric studies made by the authors show that the error made using the proposed equations, (21), (23), (24) for a square control perimeter of the same length is 1% for $T/T_{cr} = 0.25$ and 5% for $T/T_{cr} = 1$

3. Verification of the model

3.1 Experimental campaign

A total of 5 slabs of 1650 x 1650 x 120 mm were cast and tested by the authors [24]. The supporting system consisted in 8 load cells placed at the vertices of a regular octagon, equidistant 750 mm from the load application point which is on its center (Fig 9-a). The specimens were subjected to tension in their plane, in only one direction, using 10 bars of 25 mm in diameter of tensile strength f_{pu}=1050 N/mm^2 and 600 mm in length, partially embedded in two opposite faces (5 bars on each side) (Fig 9-b). These bars were connected to the tensioning system with the help of couplers and 1.5 m bar extensions that were stretched by hollow jacks, as can be seen in Fig. 9-c, to apply the tensile force in the slab. Four out of the five tested specimens were subjected to different levels of tensile stresses, whilst the control slab was left un-tensioned. The value of the external load applied during each test was defined based on the tensile force producing the cracking of the slab cross section, (i.e. $T_{cr} = A_c \cdot f_{ct}$,), with A_c being the concrete area of the cross section and f_{ct} the tensile concrete strength. Values of the applied force, support reactions, displacements at the slab center and at the supports, and strains in 32 points of the longitudinal reinforcement (24 parallel to the tensile force and 8 in the perpendicular direction at mid-span) were captured by the instrumentation during the test. The crack patterns were recorded throughout the loading process.

Figure 9

The slabs were reinforced with two steel meshes arranged on the upper and lower faces. In the direction parallel to the external tension applied, the same amount of reinforcement was placed on both faces in all the slabs (A0, A1, A2, A3, B1). This longitudinal reinforcement consisted of 12mm bars with an effective depth $d_{l,A}$ of 99 mm in type-A slabs ($\rho_{l,A}$ = 0.0111) and 16mm bars with an effective depth $d_{l,B}$ of 97 mm in type-B slabs ($\rho_{l,B}$ = 0.020). In the direction perpendicular to the applied tensile force, on the lower face, 12mm bars with an effective depth d_t 85 mm (ρ_t = 0.0129) was arranged in all cases. To cause the punching of the slab, a 145 x 145 x 30 mm steel loading plate was used. The rest of the details concerning the specimens, test set-up and instrumentation are fully described in [24], together with the description and analysis of results.

3.2 Comparison of the tests results with the predictions of the proposed model

3.2.1 Evolution of the punching shear strength

The main interest of the experimental campaign was to observe the variation of the ultimate punching shear load as a function of the tensile force applied to the slabs. For this purpose, the experimentally obtained load-displacement curves of each test were analyzed, including that of the control slab.

Predictions for punching shear failure load of each specimen have been made with the proposed model, according to Eqs. (21) and (24). The ratios between ultimate load for each test (T>0) and that of the reference test (T=0) are plotted in Fig. 10, both the experimental results and the model predictions. In addition, Table 1 shows the experimental results and the theoretical predictions of all tested slabs, using the concrete strength of each slab at the age of testing. As observed, there is only one specimen type-B which was tested with a tensile force of T/T_{cr}=0.44.

Table 1

Figure 10

As can be seen, there is a remarkable and progressive reduction in the failure load with respect to the value obtained in the control slabs. The maximum reduction was 28% for T = 1.26

404 T_{cr}. It can also be observed that the extension of the theoretical model CCCM to the punching
405 shear strength of slabs subjected to in plane tensile forces, and in particular its application to
406 unidirectional tensile forces fits very well the experimental results.

407 The decreasing trend is practically linear with the applied tensile force and is accentuated
408 in cases where the applied force is greater or equal than T_{cr}. This may occur due to the fact that
409 when T_{cr} is exceeded, cracking of the concrete occurs and, at the crack, the entire value of the
410 applied external force is resisted by the reinforcement, which increases dramatically its stress,
411 reducing its contribution to the punching shear strength.

412 This effect is captured by the model, as explained in section 2 and in Figure 8. As observed
413 in the theoretical curve calculated with the parameters of type-A slabs of Fig. 10, for values of
414 the external force close to T_{cr} = 1, the punching shear strength associated to reinforcement
415 yielding, V_y given by Eq. (24), becomes dominant over $V_{R,t}$ in the stressed direction, and for this
416 reason the slope of the curve decreases from that point onwards. A similar analysis has been made
417 for slab Type B, in which this effect is not observed, because after cracking, the remaining
418 capacity of the reinforcement $f_y^* = f_y - T/A_s$ is higher than in type-A slabs. Therefore, the
419 contribution of the longitudinal reinforcement to the punching shear strength is enough to keep
420 $V_{R,t}$ as the dominant failure load in the stressed direction.

421 **3.2.2 Strains in the reinforcement**

422 In order to study the evolution of the strains in the reinforcement at the central area of the slabs,
423 a set of strain gauges was placed on both the reinforcement parallel to the external tensile force
424 and perpendicular to it. Firstly, the data yielded by the gauges glued to the reinforcement parallel
425 to the external force was closely monitored during the tensioning stage, to ensure a homogenous
426 distribution of the tensile stresses along the mid-section of the slabs prior to the beginning of the
427 punching test.

428 During the punching test, the main goal of the strain gauges was to control the moment of
429 yielding of the reinforcement parallel to the tensile force. If yielding takes place for a punching
430 load close to the failure load, it may be assumed that yielding of the reinforcement is not
431 influencing the punching strength, and thus and $V_{R,t}$ prevails over V_y. On the other hand, if yielding

of the reinforcement takes place in an early stage of the punching test, a flexural-punching failure occurs, and V_y prevails over $V_{R,t}$.

Figure 11 shows that yielding of the longitudinal reinforcement in all the type-A slabs. In the control slab ($T=0$), yielding occurred at a load level very close to the failure load. For the case of T/T_{cr} = 0.69, the average strain in the reinforcement reached the yielding strain when the load applied was an 88% of the failure load. In the other two cases, where T/T_{cr} = 1.02 and T/T_{cr} = 1.26 the average strain in the reinforcement reached the yielding strain when the load applied was a 58% and a 42% of their respective failure loads.

Figure 11

Figure 12 shows the evolution of the average strains of the reinforcement located in the central part of the slab in both directions. In the control slab, both reinforcements presented similar values of strain during the whole test, reaching yielding for a punching load very close to the failure load. For the case of T/T_{cr} = 0.69, the slope of the force-strain curve of the perpendicular reinforcement increased a 14% when the parallel reinforcement reached yielding. This slope incremented by 11% for T/T_{cr} = 1.02 and by 14% for T/T_{cr} = 1.26.

Finally, figure 13 shows the comparison between the mean reactions measured at the load cells closest to the sides of the slab perpendicular to the external force (longitudinal reaction) and at the closest ones to the sides parallel to the external force (transverse reaction). As can be seen for values of T = 0 and T/T_{cr} = 0.69, the evolution of the reactions barely changes after the yielding of the reinforcement parallel to the external force. However for T/T_{cr} = 1.02 and T/T_{cr} = 1.26 an increment in the transverse reaction and a decrement of the longitudinal reaction with respect to the mean reaction occurs, more accentuated in the case of T/T_{cr} = 1.26

These behaviors may indicate that there was a moment redistribution process in the specimens subjected to high axial load levels, which may occur without collapse due to the static indeterminacy of two way slabs. In summary, the observed experimental behavior corroborates

459 the assumptions of the model related to the effects of the in-plane tensile forces on the punching
460 shear strength.
461
462 Figure 12
463
464 Figure 13
465
466 ## 4. Predictions of the tests results using several design codes provisions
467 Table 3 compares the punching-shear strength predictions of all slabs tested by the authors, the
468 ones tested at Cornell University [16-17] and two of those tested by Regan (BD-6 and BD-8,
469 control slab) [18], using the simplified proposal presented in Section 2 and three current structural
470 codes. All safety factors have been removed from the original formulations, and reported mean
471 values of the materials strength and the actual applied loads have been used. The main
472 characteristics of Regan's and Cornell's slabs are summarized in Table 2 and Fig. 14. Regan's
473 specimens were 1.5 m square and 125 mm thick (Fig. 14-a) and have been considered simply
474 supported on their four sides for the calculations, despite the testing set up may have introduced
475 some restriction to the rotation at the supports. Cornell's specimens were 1.2 m square and 150
476 mm thick simply supported on their four sides (Fig 14-b).
477
478 Table 2
479
480 Figure 14
481
482 EC-2 [20] predictions are made using the equation presented in section 6.4.4 (1), which
483 accounts for the effects of normal stresses with the additive term σ_{cp}. Regarding ACI, the
484 formulation presented in section 11.12.2.3 of ACI 349-06 [22] has been selected (3) rather than
485 the formula of section 22.5.7 (2) of ACI 318-14 [21], which yielded highly conservative results.
486 Finally, Level of Approximation II has been used for MC-2010 [23] predictions. In this case, the

effects of tensile stresses have been introduced in the calculation of the slab's rotation ψ, Eq. (25), through term m_{Rd}, which has been calculated taking account of the applied tensile force.

$$\psi = 1.5 \cdot \frac{r_s}{d}\frac{f_y}{E_s} \cdot \left(\frac{m_{Ed}}{m_{Rd}}\right)^{1.5} \tag{25}$$

To calculate the term m_{Ed}, the equation (7.3-71) of MC-2010 has been used, considering no eccentricity of the resultant of the shear forces with respect to the centroid of the control perimeter. Therefore, $m_{Ed} = V_{Ed}/8$, being V_{Ed} actually the punching strength of each slab ($V_{Ed} = V_{Rd}$). Thus, Eq. (26) has been solved iteratively for each value of the external applied load.

$$V_{Rd} = \frac{1}{1.5 + 0.9k_{dg} \cdot d \cdot 1.5 \cdot \frac{r_s}{d}\frac{f_y}{E_s} \cdot \left(\frac{\frac{V_{Rd}}{8}}{m_{Rd}}\right)^{1.5}} \sqrt{fc} \cdot b_0 \cdot d \tag{26}$$

Regarding the ultimate load prediction using the codes provisions, in uniaxial tension, best results are yielded by EC-2, followed closely by MC-2010, whereas for biaxial tension, best results are yielded by MC-2010, followed by EC-2, whereas ACI 349-06 yields more conservative results in both cases. As far as CCCM concerns, it seems to be the best prediction method for uniaxial tension. Unfortunately, the available database of this type of tests is scarce, and needs to be extended with future research on this topic. For biaxial tension both CCCM and MC-2010 yield similar average results ($\frac{P_{exp}}{P_{model}} = 1.26$ and 1.21 respectively), but CCCM has a slightly lower coefficient of variation than MC-2010 (9.76 % and 12.72 % respectively). Globally, best results are given by the CCCM with an average value of $\frac{P_{exp}}{P_{model}}$ =1.11 and a coefficient of variation of 9.32%, with a minimum value of 0.939 and a maximum value of 1.498. Table 3, along with Fig. 15 summarize the results of the comparison.

Table 3

Figure 15

5. CONCLUSIONS

A mechanical model for the shear punching strength of RC flat slabs subjected simultaneously to concentrated loads and in-plane tensile forces, has been described and verified with the results of previously carried out experimental campaigns. The developed model has been derived from the Compression Chord Capacity Model for punching shear, by identifying the main effects of in-plane tensile forces on the punching shear resisting mechanisms and failure modes, and incorporating them into their governing equations. The following main conclusions can be drawn from the studies performed:

1. The following main effects of in-plane tensile forces on the punching shear strength of slabs, have been identified:
    a. A reduction of the neutral axis depth, and the corresponding reduction of the contribution of the compression chord to the shear strength.
    b. An increment of the tension in the longitudinal reinforcement and, by equilibrium, a decrement of compression stress in the un-cracked concrete chord, thus reducing its shear transfer capacity.
    c. A possible premature cracking of concrete, due to a high level of pure tension, that considerably increases the tensile stress in the longitudinal reinforcement.
    d. An increment of the critical crack width, that reduces the transfer capacity of shear and residual tensile stresses, along the crack.
2. Simple and accurate design equations have been derived, showing that the shear transfer capacity of the compressed chord linearly decreases as a function of the ratio T/T_{cr}, where T is the applied tensile force and T_{cr} is the force that produces cracking in the concrete.
3. The model has been able to accurately reproduce the results of an experimental campaign carried out by the authors, on 5 slabs subjected to a concentrated load and different levels of unidirectional in-plane tensile forces. The experimentally observed behaviour has been captured both qualitatively and quantitatively, with an average error on the prediction of the ultimate load of 5%.
4. When a high tensile force T is applied, the increment of tensile stress in the longitudinal reinforcement due to the tensile force may be such that yielding of the reinforcement

under increasing concentrated load may occur prior to punching failure, thus reducing the punching strength. Such phenomenon usually occurs for $T>T_{cr}$. However, for low reinforcement ratios, it can also occur for $T<T_{cr}$.

5. The above described phenomenon is captured by the model, in which such failure is associated to the load that produces yielding in the flexural reinforcement in both directions, when yielding takes place. The relationship between the ultimate load and the ratio T/T_{cr} results approximately bilinear, with higher slope when premature yielding of the longitudinal reinforcement takes place.
6. If additional reinforcement is placed to resist the applied tensile force, even in case that the section cracks ($T>T_{cr}$), the increment of stress in the longitudinal reinforcement may not be enough to produce yielding prior to the punching failure, thus contributing to avoid the "extra" reduction of punching strength.
7. Predictions of punching-shear-tension tests results, available in the literature, were made with the proposed CCCM model and with different theoretical models included in design codes (EC-2, ACI 349-06, MC-2010 (LoA II)). It was showed that the best results are yielded by the proposed model (mean error of 5.3% (CoV=2.85%) for the case of uniaxial tension and 12.6% (CoV=9.76%) for biaxial tension. Among the Codes provisions, EC-2, provides the best predictions for uniaxial tension (mean error of 13.5% (CoV=4.71%) whereas MC-2010 provides the best results for biaxial tension (mean error of 12.1% and CoV=12.72%). Mostly all the predictions of the ultimate load are conservative, being the ACI 349-06 predictions the most conservative ones.

Acknowledgements

This work was developed in the framework of Research Project BIA-2015-64672-C4-1-R, financed by the Ministry of Economy and Competitiveness (MINECO) of Spain and the European Funds for Regional Development (FEDER). The authors want to thank Mr. José Romo, from FHECOR Engineering, for transmitting his experience in bridge design that helped to set the

problem and to the director and technicians of the Structural Technology Laboratory of UPC, for their help in carrying out the experimental campaign.

References

[1] Kinnunen S, Nylander H. Punching of concrete slabs without shear reinforcement. Transactions No. 158; Royal Institute of Technology; Stockholm: 1960.

[2] Braestrup MW, Nielson MP, Jensen BC, Bach F. Axisymmetric Punching of Plain and Reinforced Concrete. vol. 75. Structure Research Laboratory, Technical University of Denmark: 1976.

[3] Regan PE, Braestrup MW. Punching shear in reinforced concrete: a state-of-art report. CEB Bulletin d'Information 168, Lausanne: Comité euro-international du béton; 1985.

[4] Bazant ZP, Cao Z. Size Effect in Punching Shear Failure of Slabs. ACI Struct J 1987;84:44–53. doi:10.14359/2785.

[5] Broms CE. Punching of flat plates. A question of concrete properties in biaxial compression and size effect. ACI Struct J. 1990;87:292–304. doi:10.14359/2624.

[6] Bortolotti L. Punching Shear Strength in Concrete Slabs. ACI Struct J 1991;87:208–19. doi:10.14359/2717.

[7] Hallgren M. Punching shear capacity of reinforced high strength concrete slabs. KTJ Stockholm, TRITA-BKN. Bull.9, 1994.

[8] Fédération Internationale du Béton (fib). Punching of structural concrete slabs. Bulletin12. Lausanne: International Federation for Structural Concrete; 2001.

[9] Menétrey P. Analytical Model for punching strength prediction. Int. Work. Punching Shear Capacit. RC Slabs, Stockholm: 2000, p. 190–9.

592 [10] Polak MA. SP-232: Punching Shear in Reinforced Concrete Slabs. Am. Concr. Institute,
593 Spec. Publ., vol. 232, 2005, p. 302. doi:10.14359/14960.
594 [11] Muttoni A. Punching shear strength of reinforced concrete slabs without transverse
595 reinforcement. ACI Struct J 2008;105:440–50.
596 [12] Park H-G, Choi K-K, Chung L. Strain-based strength model for direct punching shear of
597 interior slab–column connections. Eng Struct 2011;33:1062–73.
598 doi:10.1016/J.ENGSTRUCT.2010.12.032.
599 [13] Koppitz R, Kenel A, Keller T. Punching shear of RC flat slabs – Review of analytical
600 models for new and strengthening of existing slabs. Eng Struct 2013;52:123–30.
601 doi:10.1016/J.ENGSTRUCT.2013.02.014.
602 [14] Guandalini S, Burdet OL, Muttoni A. Punching Tests of Slabs with Low Reinforcement
603 Ratios. ACI Struct J 2009;106:87–95. doi:10.14359/56287.
604 [15] Kueres D, Siburg C, Herbrand M, Classen M, Hegger J. Uniform Design Method for
605 punching shear in flat slabs and column bases. Eng Struct 2017;136:149–64.
606 doi:10.1016/J.ENGSTRUCT.2016.12.064.
607 [16] Abrams, J.H. The Punching Shear Strength of Pre-cracked Reinforced Concrete in Biaxial
608 Tension", M.S. Thesis Cornel University, May 1979.
609 [17] Jau, W.C, White. R.N, Gergely, P. Behavior of reinforced concrte slabs subjected to
610 combined punching and biaixal tension. Report for U.S. Nuclear Regulatory Comission,
611 1982
612 [18] Regan, P.E. Punching shear in prestressed concrete slab bridges. Engineering Structures
613 Research Group, Polytechnic of Central London, 1983.
614 [19] Bui TT, Nana WSA, Abouri S, Liman A, Tedoldi B, Roure T. Influence of uniaxial tension
615 and compression on shear strength of concrete slabs without shear reinforcement under
616 concentrated loads. Construction and Building Materials 2017:147;86-101
617 [20] European Committee for Standardization. Eurocode 2: design of concrete structures: Part
618 1: general rules and rules for buildings. Brussels, Belgium: European Committee for
619 Standardization; 2002

620 [21] ACI 318-14. Building code requirements for structural concrete and commentary.
621 American Concrete Institute, 2014
622 [22] ACI 349-06. Code Requirements for Nuclear Safety Concrete Structures. American
623 Concrete Institute, 2007
624 [23] Fédération international du Béton. Fib Model Code for Concrete Structures 2010 vol. 1.
625 Lausanne: Ernst & Sohn; 2013
626 [24] Fernandez, P.G., Marí A, Oller E. " (2020) "Punching shear strength of reinforced concrete
627 slabs subjected to unidirectional in-plane tensile forces, Structural Concrete, FIB,
628 Accepted for publication. DOI: 10.1002/SUCO.202000112
629 [25] Marí A, Cladera A, Oller E, Bairán JM. A punching shear mechanical model for reinforced
630 concrete flat slabs with and without shear reinforcement. Engineering Structures
631 2018:166;413-26
632 [26] Cladera, A., Marí, A., Bairán, JM. Oller, E., Duarte, N. (2016) "The compression chord
633 capacity model for the shear design and assessment of reinforced and prestressed concrete
634 beams" Structural Concrete (FIB), Wiley, 18-2, pp1017-1032, ISSN 1464-4177
635 [27] Marí A, Bairán J, Cladera A, Oller E, Ribas C. Shear-flexural strength mechanical model
636 for the design and assessment of reinforced concrete beams. Struct Infrastruct Eng
637 2015;11:1399–419. doi:10.1080/15732479.2014.964735.
638 [28] Walraven, J.C. Fundamental analysis of agreggate interlock. Journal of the structural
639 division-ASCE, 1981; 107(11), 2245-2270.
640 [29] Vecchio, F.J., Collins, M.P. The modified compression field theory for reinforced-
641 concrete elements subjected to shear. Journal of the American Concrete Institute, 1986;
642 83(2), 219-231.
643 [30] Kupfer, H. B. and Gerstle, K. H. Behavior of concrete under biaxial stresses. J Eng Mech
644 Div, 1973; 99, 853–866.
645 [31] Marí A, Cladera A, Bairán JM. Effects of axial forces and prestressing on the shear
646 strength of structural concrete member . Proceedings, VII International Structures

Conference, Spanish Ass. of Structural Engineering, ACHE, A Coruña, Spain. June, 2017.

[32] Sagaseta J, Muttoni A, Fernández Ruiz M, Tassinari L. Non-axis symmetrical punching shear around internal columns of RC slabs without transverse reinforcement. Magazine of concrete research, Paper 1000098, Nº3, 17p, 2011

List of Figures

681 List of Tables

682

686

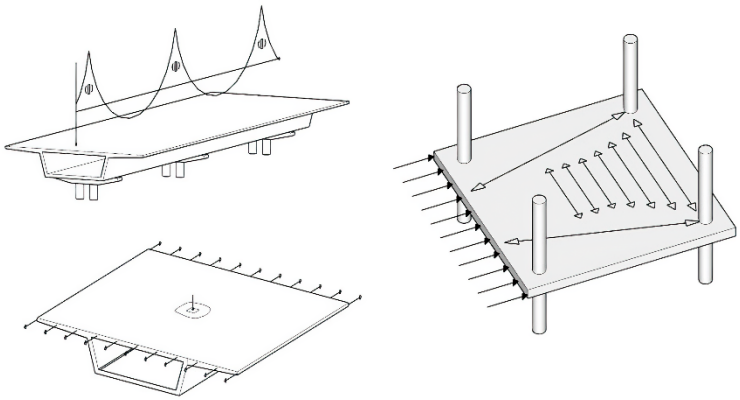

687

688 **Fig. 1.** Common situations where in-plane tensile stresses and a concentrated load may act together.

689

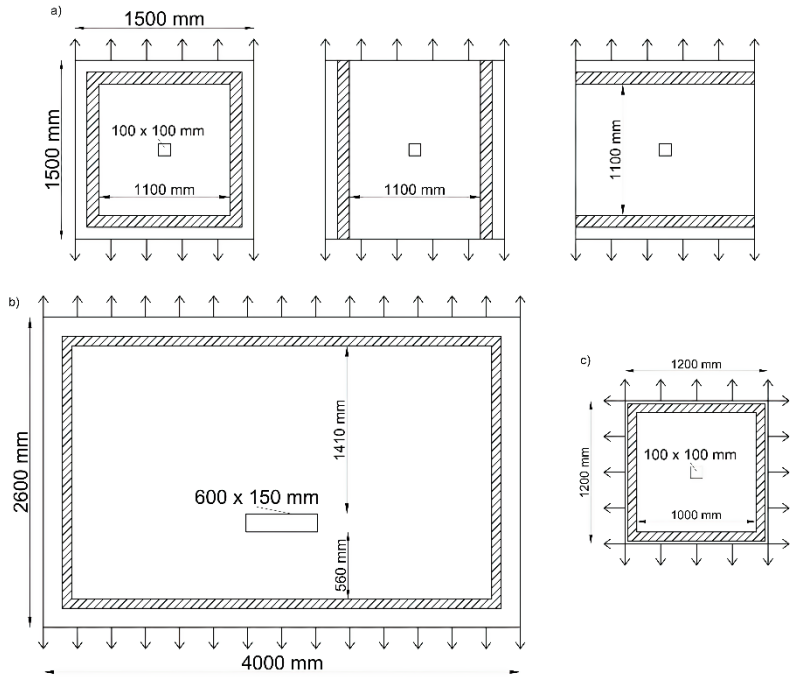

690

691 **Fig. 2.** Set-up of the tests carried out by a) Regan [18] b) at the University of Lyon [19] c) at Cornell

692 University [16-17].

693

694

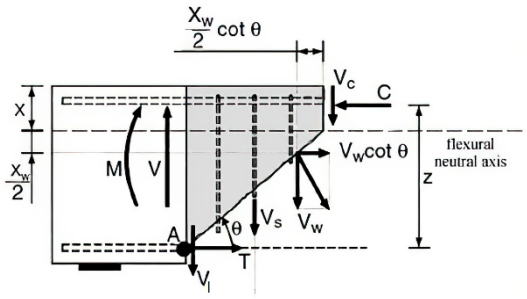

695 **Fig. 3**. Shear transfer mechanism and scheme of equilibrium of the considered forces in the shear model.

696

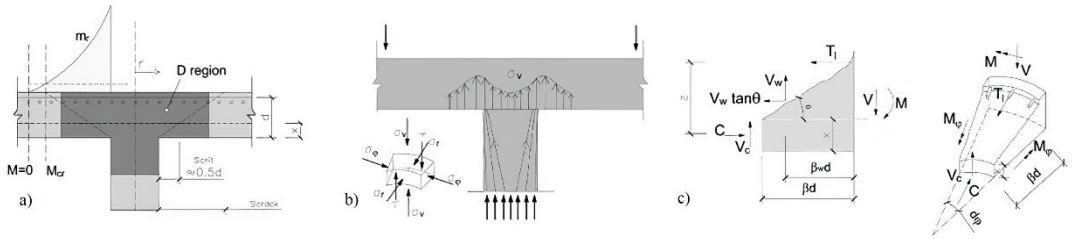

Fig. 4. a) Position of the control perimeter. b) Vertical stresses in the vicinity of the column c) Shear transfer actions and scheme of equilibrium of the considered forces in the punching model.

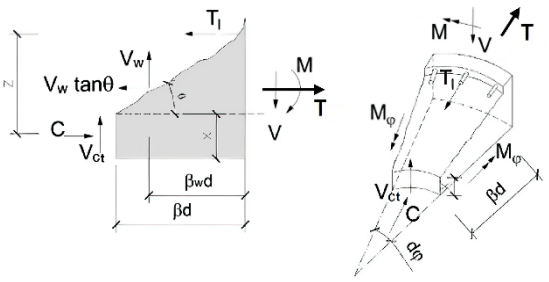

Fig. 5. Equilibrium of forces in a differential slice of slab, including in-plane tensile forces.

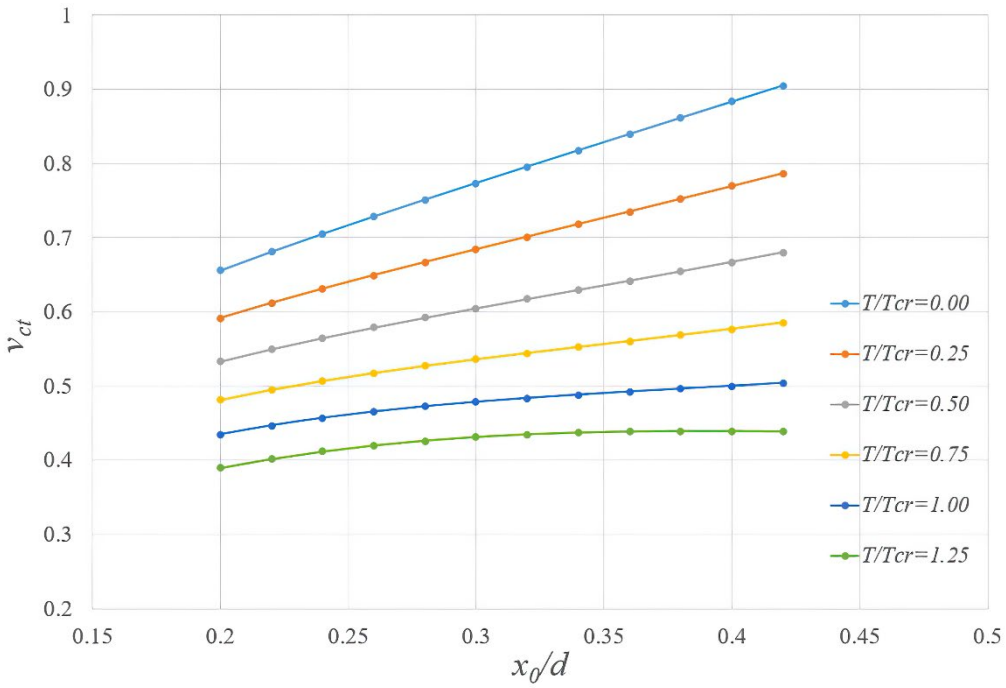

704

705 **Fig. 6**. Dimensionless shear carried by the un-cracked chord v_{ct} for different values of T/T_{cr}.

706

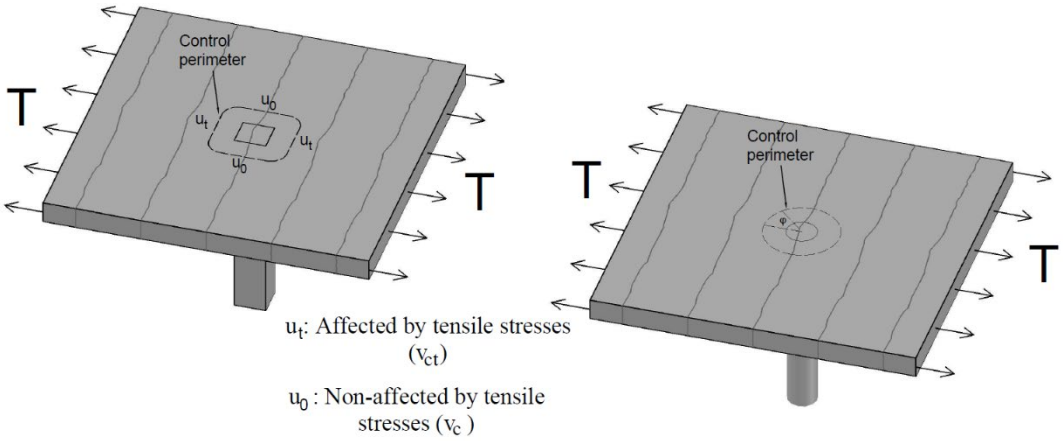

707

708 **Fig. 7.** Parts of the control perimeter affected and non-affected by tensile stresses.

709

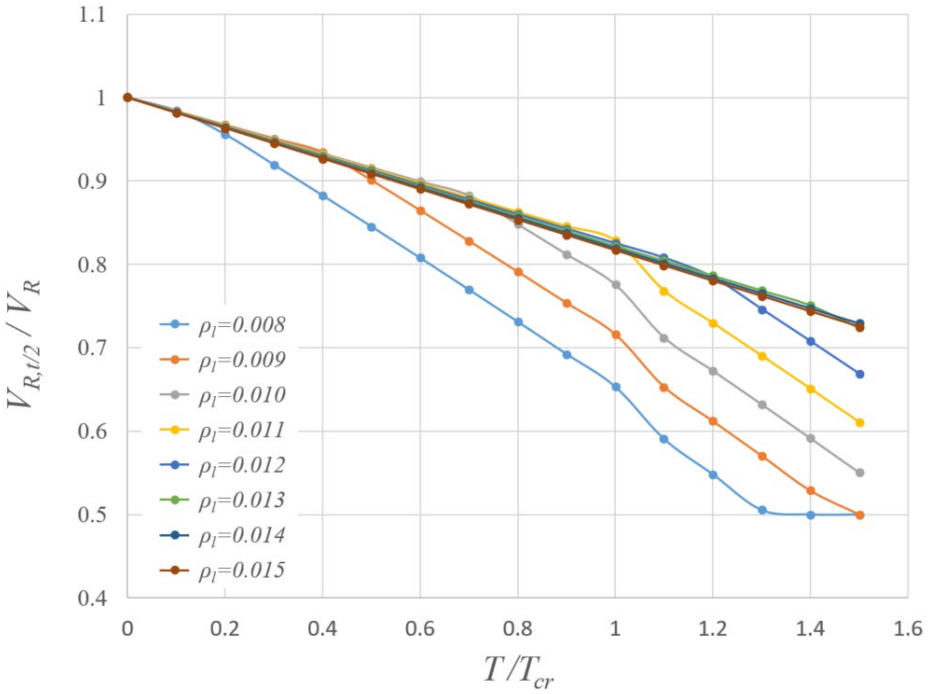

710

711 **Fig. 8.** Influence of ρ_l on the reduction of shear punching strength as T/T_{cr} increases for the unidirectional

712 tension case.

713

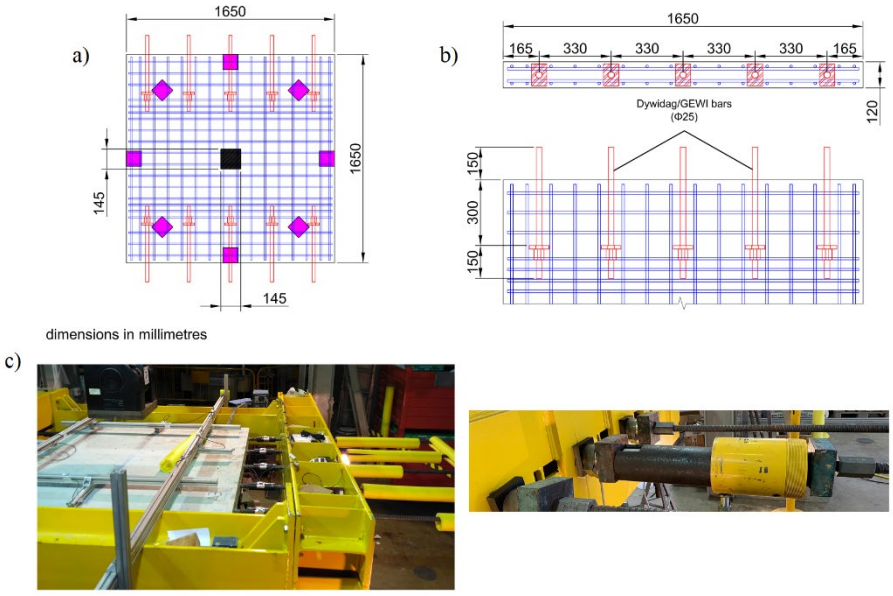

Fig. 9. a) Support scheme. b) Position of the bars used to introduce tensile forces in the slab. c) Tensioning system

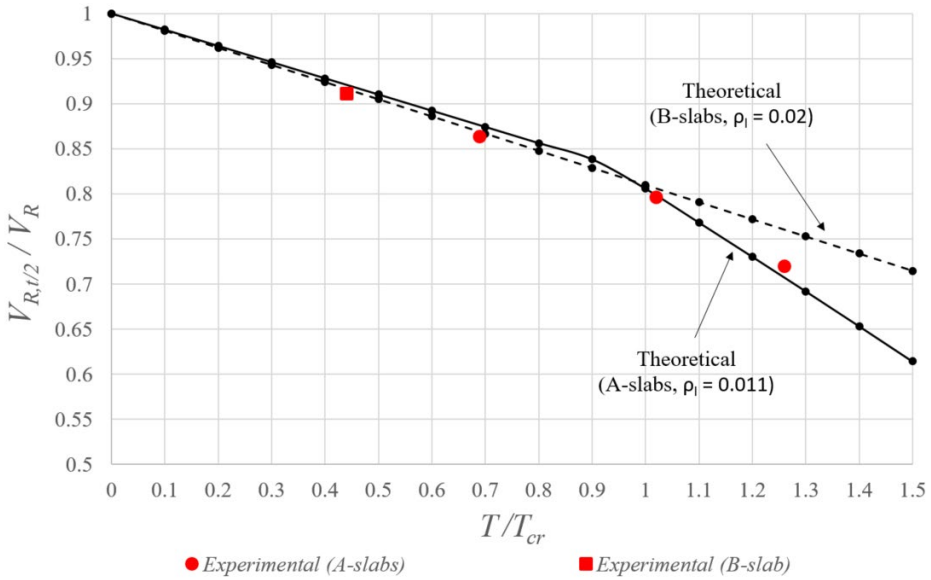

719

720 **Fig. 10.** Theoretical and experimental punching shear strength vs. relative tensile force applied T/T_{cr}

721

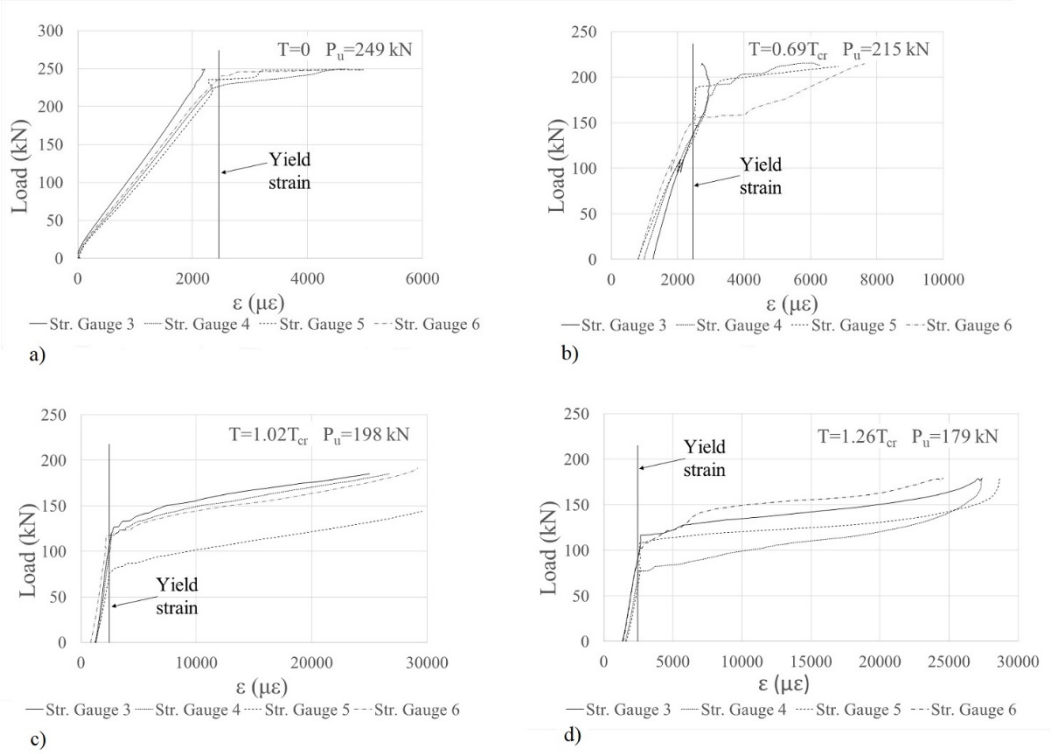

Fig. 11. Evolution of strains in the longitudinal reinforcement: a) T=0; b) T=0.69T_{cr}; c) T=1.02T_{cr}; d) T=1.26T_{cr}.

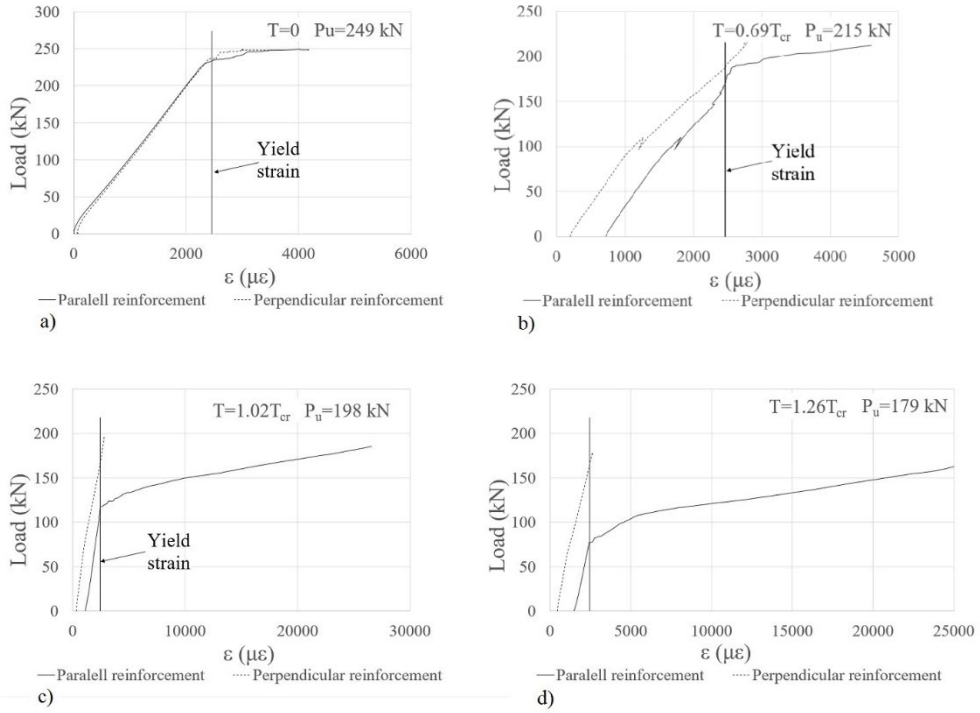

726

727 **Fig. 12.** Relation between strains in the reinforcement parallel and perpendicular to the tensile force. a)

728 T=0; b) T=0.69T_{cr}; c) T=1.02T_{cr}; d) T=1.26T_{cr}.

729

730

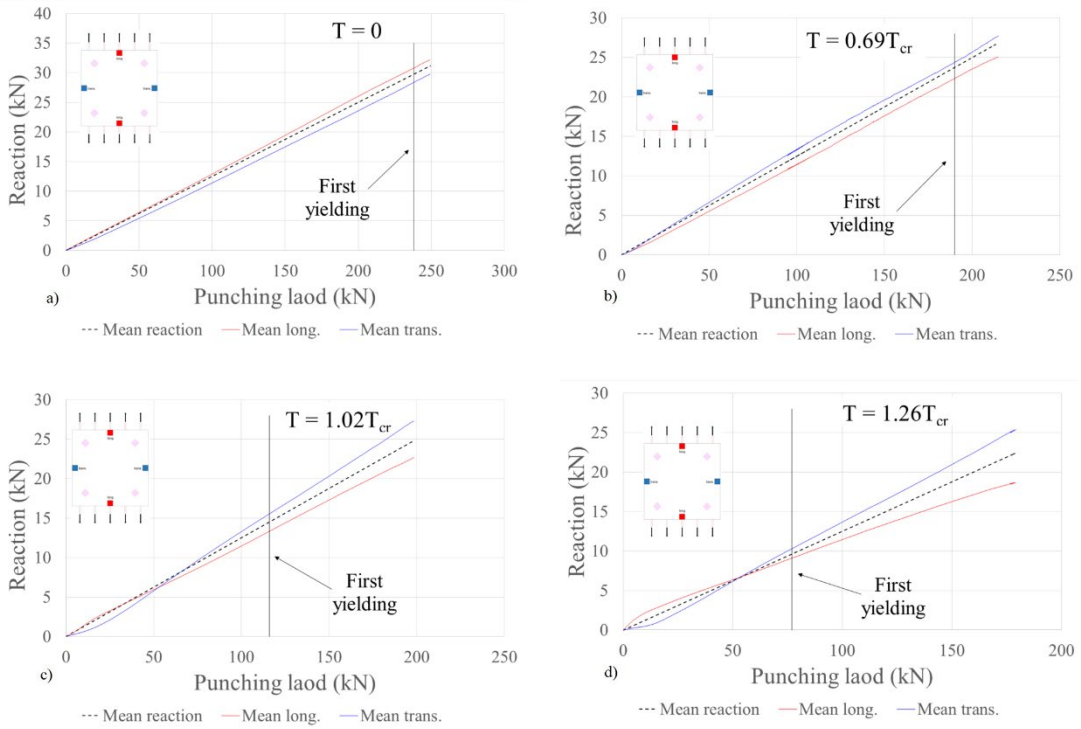

731
732 **Fig. 13.** Evolution of the longitudinal and transverse reaction during the tests. a) T=0; b) T=0.69T_{cr}; c)
733 T=1.02T_{cr}; d) T=1.26T_{cr}.

734

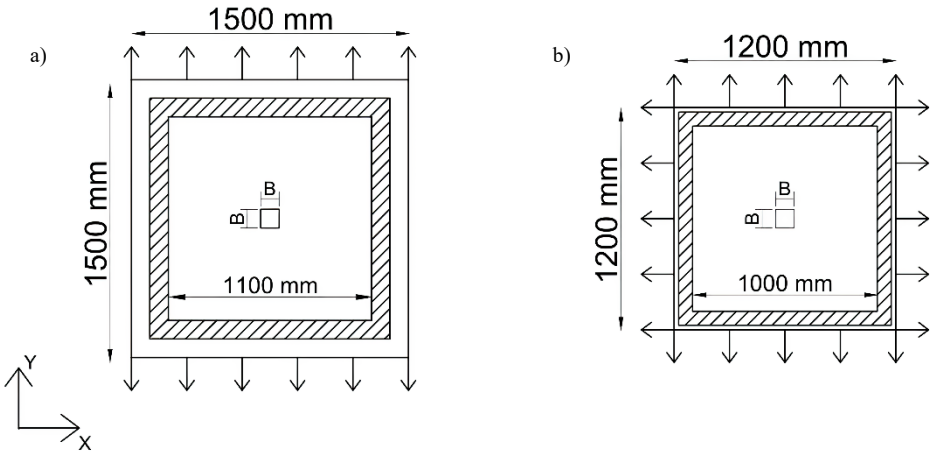

735

736 **Fig. 14.** a) Regan's and b) Cornell's slabs dimensions.

737

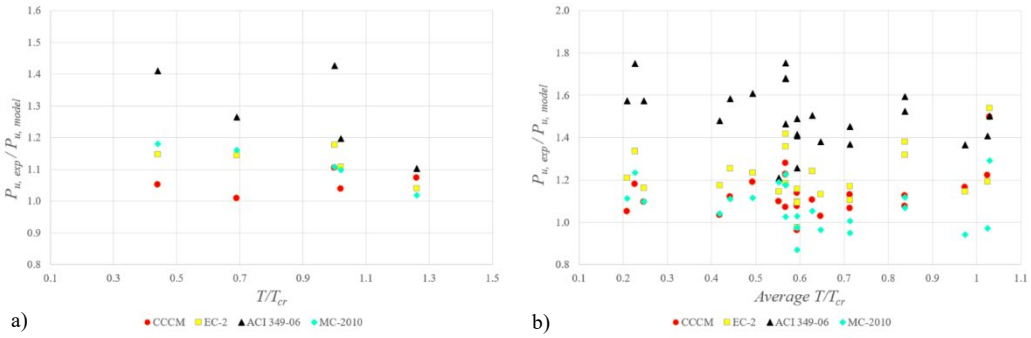

Fig. 15. Comparison of ultimate loads obtained with each design method. a) Uniaxial tension b) Biaxial tension

742 **Table 1.** Test results and theoretical predictions with the proposed model

Slab	T/T_{cr}	$f_{c,cyl}$ (MPa)	f_{ct} (MPa)	Experim. P_u (kN)	Theoret. P_u (kN)	P_{uexp}/P_{theo}	Experim. $P_u/P_{control}$	Theoret. $P_u/P_{control}$
A1	0.00	37.6	3.38	249.1	242.1	1.029	1	1
B1	0.44	37.7	3.41	240.4	233.2	1.031	0.911	0.915
A2	0.69	35.9	3.05	215.2	210.6	1.023	0.864	0.870
A3	1.02	37.4	3.13	198.4	196.1	1.012	0.796	0.813
A4	1.26	36.7	3.36	179.4	171.9	1.044	0.720	0.710

743

744

745 **Table 2.** Regan's and Cornell's slabs characteristics (Figure 14)

	Slab	$f_{c,cyl}$ (MPa)	f_{ct} (MPa)	B (mm)	d_X (mm)	d_Y (mm)	ρ_X (%)	ρ_Y (%)	T/T_{cr} X	T/T_{cr} Y
REGAN	BD-6	38.9	3.2	100	95	107	1.360	1.208	1.00	0
	BD-8	39.7	2.7	100	95	107	1.360	1.208	0	0
CORNELL	00B8	22.3	NR	200	108.7	116.6	1.585	0.720	0.00	0.00
	08B8	22.6	NR	200	108.7	116.6	1.585	0.720	1.37	0.69
	00C4	21.7	NR	100	115.1	116.6	0.680	0.380	0.00	0.00
	08C4	23.4	NR	100	115.1	116.6	0.680	0.380	0.69	0.41
	00D8	22.9	NR	200	108.7	116.6	1.585	0.720	0.00	0.00
	09A	28.3	NR	100	108.7	116.6	1.585	0.720	0.76	0.38
	09B	28.3	NR	100	108.7	116.6	1.585	0.720	0.76	0.38
	09C	28.3	NR	100	108.7	116.6	1.585	0.720	0.76	0.38
	09D	28.3	NR	100	108.7	116.6	1.585	0.720	0.76	0.38
	06A	22.1	NR	100	108.7	116.6	1.585	0.720	0.79	0.40
	06B	22.1	NR	100	108.7	116.6	1.585	0.720	0.79	0.40
	06C	22.1	NR	100	108.7	116.6	1.585	0.720	0.79	0.40
	06D	22.1	NR	100	108.7	116.6	1.585	0.720	0.79	0.40
	06E	24.1	NR	100	108.7	116.6	1.585	0.720	0.95	0.48
	06F	24.1	NR	100	108.7	116.6	1.585	0.720	0.95	0.48
	00A	31.0	NR	100	108.7	116.6	1.585	0.720	0.00	0.00
	00B	31.0	NR	100	108.7	116.6	1.585	0.720	0.00	0.00
	09E	31.0	NR	100	108.7	116.6	1.585	0.720	1.12	0.56
	09F	31.0	NR	100	108.7	116.6	1.585	0.720	1.12	0.56
	00C	28.3	NR	100	108.7	116.6	1.585	0.720	0.00	0.00
	02A	28.3	NR	100	108.7	116.6	1.585	0.720	0.30	0.15
	04A	28.3	NR	100	108.7	116.6	1.585	0.720	0.59	0.30
	06G	28.3	NR	100	108.7	116.6	1.585	0.720	0.86	0.43
	00D	29.7	NR	100	108.7	116.6	1.585	0.720	0.00	0.00
	02B	29.7	NR	100	108.7	116.6	1.585	0.720	0.28	0.14
	04B	29.7	NR	100	108.7	116.6	1.585	0.720	0.56	0.28
	06H	29.7	NR	100	108.7	116.6	1.585	0.720	0.84	0.42
	02C	22.7	NR	100	108.7	116.6	1.585	0.720	0.33	0.17
	04C	22.7	NR	100	108.7	116.6	1.585	0.720	0.66	0.33
	08A	22.7	NR	100	108.7	116.6	1.585	0.720	1.29	0.65
	08B	22.7	NR	100	108.7	116.6	1.585	0.720	1.36	0.69

746 **NR**: Not reported

747

748

749

750

751

752

753 **Table 3.** Comparison of the ultimate load predictions. (Figure 15)

Type	Slab	T/T_{cr} X	T/T_{cr} Y	$f_{c,cyl}$ (MPa)	$P_{u,exp}$ (kN)	P_{exp}/P_{CCCM}	P_{exp}/P_{EC2}	P_{exp}/P_{ACI}	P_{exp}/P_{MC10}
UNIAXIAL TENSION	A1	0	0	37.6	249.1	1.048	1.205	1.423	1.280
	BD-8	0	0	39.7	251.0	1.048	1.119	1.482	1.176
	B1	0.44	0	37.7	240.4	1.052	1.147	1.409	1.181
	A2	0.69	0	35.9	215.2	1.008	1.145	1.265	1.160
	BD-6	1.00	0	38.9	225.0	1.038	1.108	1.196	1.098
	A3	1.02	0	37.4	198.4	1.105	1.178	1.427	1.108
	A4	1.26	0	36.7	179.4	1.074	1.040	1.102	1.019
BIAXIAL TENSION	00B8	0.00	0.00	22.3	400.8	1.283	1.534	1.786	1.506
	08B8	1.37	0.69	22.6	306.0	1.498	1.539	1.503	1.290
	00C4	0.00	0.00	21.7	223.3	1.139	1.155	1.290	1.244
	08C4	0.69	0.41	23.4	185.0	1.098	1.145	1.209	1.189
	00D8	0.00	0.00	22.9	375.1	1.201	1.436	1.671	1.410
	09A	0.76	0.38	28.3	279.5	1.280	1.418	1.753	1.228
	09B	0.76	0.38	28.3	267.4	1.225	1.357	1.678	1.175
	09C	0.76	0.38	28.3	267.9	1.227	1.359	1.680	1.177
	09D	0.76	0.38	28.3	233.6	1.070	1.186	1.466	1.026
	06A	0.79	0.40	22.1	200.7	1.081	1.099	1.415	0.978
	06B	0.79	0.40	22.1	211.4	1.138	1.158	1.490	1.030
	06C	0.79	0.40	22.1	178.4	0.961	0.977	1.258	0.870
	06D	0.79	0.40	22.1	199.8	1.076	1.094	1.408	0.974
	06E	0.95	0.48	24.1	199.8	1.067	1.104	1.369	0.949
	06F	0.95	0.48	24.1	211.8	1.131	1.171	1.452	1.007
	00A	0.00	0.00	31.0	296.8	1.068	1.255	1.675	1.196
	00B	0.00	0.00	31.0	310.2	0.977	1.312	1.750	1.250
	09E	1.12	0.56	31.0	245.2	1.077	1.320	1.524	1.069
	09F	1.12	0.56	31.0	256.3	1.126	1.380	1.593	1.117
	00C	0.00	0.00	28.3	298.2	0.939	1.300	1.761	1.251
	02A	0.30	0.15	28.3	289.3	1.180	1.336	1.749	1.234
	04A	0.59	0.30	28.3	255.9	1.121	1.253	1.583	1.111
	06G	0.86	0.43	28.3	218.1	1.028	1.133	1.380	0.965
	00D	0.00	0.00	29.7	285.2	1.053	1.224	1.644	1.172
	02B	0.28	0.14	29.7	267.0	1.052	1.209	1.574	1.114
	04B	0.56	0.28	29.7	245.2	1.035	1.176	1.479	1.041
	06H	0.84	0.42	29.7	243.4	1.106	1.241	1.504	1.055
	02C	0.33	0.17	22.7	233.6	1.097	1.162	1.575	1.098
	04C	0.66	0.33	22.7	233.2	1.191	1.234	1.608	1.115
	08A	1.29	0.65	22.7	189.1	1.165	1.144	1.366	0.943
	08B	1.36	0.69	22.7	194.0	1.223	1.192	1.408	0.972
	Mean Uniaxial					1.053	1.135	1.329	1.146
	CoV Uniaxial (%)					2.847	4.706	10.705	7.150
	Max.					1.105	1.205	1.482	1.280
	Min.					1.008	1.040	1.102	1.019
	Mean Biaxial					1.126	1.245	1.535	1.121
	CoV Biaxial (%)					9.757	10.480	10.283	12.718
	Max.					1.498	1.539	1.786	1.506
	Min.					0.939	0.977	1.209	0.870
	Total Mean					1.113	1.225	1.497	1.126
	Total CoV (%)					9.320	10.380	11.577	11.808

754
755